Arch. Metall. Mater. **66** (2021), 3, 803-808

DOI: 10.24425/amm.2021.136384

P. SHARIEF[1], B. MADAVALI[1], Y. SOHN[2], J.H. HAN[2], G. SONG[1], S.H. SONG[1], S.J. HONG[1*]

REDUCTION OF THERMAL CONDUCTIVITY THROUGH COMPLEX MICROSTRUCTURE BY DISPERSION OF CARBON NANOFIBER IN P-TYPE $Bi_{0.5}Sb_{1.5}Te_3$ ALLOYS

The influence of nano dispersion on the thermoelectric properties of Bi_2Te_3 was actively investigating to wide-spread thermoelectric applications. Herein this report, we have systematically controlled the microstructure of $Bi_{0.5}Sb_{1.5}Te_3$ (BST) alloys through the incorporation of carbon nanofiber (CNF), and studied their effect on thermoelectric properties, and mechanical properties. The BST/x-CNF (x-0, 0.05, 0.1, 0.2 wt.%) composites powder was fabricated using high energy ball milling, and subsequently consolidated the powder using spark plasma sintering. The identification of CNF in bulk composites was analyzed in Raman spectroscopy and corresponding CNF peaks were recognized. The BST matrix grain size was greatly reduced with CNF dispersion and consistently decreased along CNF percentage. The electrical conductivity was reduced and Seebeck coefficient varied in small-scale by embedding CNF. The thermal conductivity was progressively diminished, obtained lattice thermal conductivity was lowest compared to bare sample due to induced phonon scattering at interfaces of secondary phases as well as highly dense fine grain boundaries. The peak *ZT* of 0.95 achieved for 0.1 wt.% dispersed BST/CNF composites. The Vickers hardness value of 101.8 Hv was obtained for the BST/CNF composites.

Keywords: Bismuth telluride, Carbon nano fiber, Grain size, Thermal conductivity, *ZT*

1. Introduction

Recent decades witnessing an increasing energy demand and expected from 2006-2030, it rises about 44% and causing global warming. Green energy from reliable, and clean energy systems were attracting considerably [1]. Thermoelectric (TE) a revolutionary technique directly converts heat energy to power generation long been used for space power and recently implemented in car exhaust waste heat into electricity [2]. The thermoelectric module performance depends on dimensionless figure of merit, $ZT = \sigma\alpha^2 T/\kappa$. Where σ, α, κ, and T were electrical conductivity, Seebeck coefficient, thermal conductivity, and corresponding temperature. The discrepancy dependent thermoelectric properties ($\sigma \propto 1/\alpha \propto 1/\kappa$) hinder the elevation of *ZT* value. The TE potential advantages stimulates researchers to improve *ZT* with novel approaches and enhances the *ZT*.

Among various TE materials, bismuth telluride (Bi_2Te_3) alloys were dominant room temperature commercial industry with its high *ZT* value [3,4]. Basically, bismuth (Bi) shows metallic behavior, with tellurium (Te) acts as a semiconductor compound used in thermoelectric refrigeration and power generators. Due to room temperature advantages, it is implemented in state-of-art applications like computer chip cooling [5], chip sensing [6]. Thermoelectric materials with high *ZT* are ideal to obtain high energy conversion. Low dimensional material capable of improving power factor in thermoelectric materials through energy filtering effect and effectively enhances the phonon scattering to minimize thermal conductivity [7-11]. Energy filtering effect was successfully obtained by Sabarinathan et al. [8] through enhancing mobility, Seebeck coefficient and power factor improved from 10 $\mu W/mK^2$ to 75 $\mu W/mK^2$. The suppression of bipolar thermal conductivity and achieving peak *ZT* at higher temperature in literatures [10,11]. The electrical conductivity and the electric thermal component (κ_e) are strongly inseparable. Hence, reducing thermal conductivity through phonon scattering is the plausible route without deteriorating electronic components. The concept for decoupling thermoelectric parameters and reducing thermal conductivity was suggested by Dresselhaus and Hickes [12] through low-dimensional materials.

Among different low-dimensional materials, carbon based nanostructures were highly investigated due to their peculiar structural, thermal, mechanical, optical, and electrical properties.

[1] KONGJU NATIONAL UNIVERSITY, DIVISION OF ADVANCED MATERIALS ENGINEERING & INSTITUTE FOR RARE METALS, CHEONAN, 331-717, REPUBLIC OF KOREA
[2] CHUNGNAM NATIONAL UNIVERSITY, DEPARTMENT OF MATERIALS SCIENCE & ENGINEERING, DAEJEON, 34134, REPUBLIC OF KOREA

* Corresponding author: hongsj@kongju.ac.kr

Their ability to chemically alter their nanostructures to enhance their solubility attracted its usage in various sectors like sensors [13], medicine [14], composite materials [15], and semiconductor devices [16]. Carbon nanostructure, carbon nanofiber (CNF) forms when graphene sheets curve at some angle to arrange as stacked nano cones. The advantages of CNF over CNT is easier to disperse, process and functionlize, cost-effective, and available in large amount/year than CNT [13-17]. Therefore, we used CNF as a secondary phase in BST matrix and its influence was studied through thermoelectric measurements and microstructure investigations.

2. Experimental procedure

The required elementals (5N) for the preparation of $Bi_{0.5}Sb_{1.5}Te_3$ (BST) were brought from the Alfa Aesar company. They were weighted accordingly $Bi_{0.5}Sb_{1.5}Te_3$ composition and fabricated using water atomization technique. The powder seived under 200 μm and carbon nanofiber (CNF) was used as a dispersant phase. The BST/CNF composites was started by weighing the BST and CNF (0, 0.05, 0.1, 0.2 wt.%) and filled in zirconium jars with zirconium balls (15:1 BPR) in argon medium, milled using 800 rpm for 20 min. Resultant powders were consolidated using spark plasma sintering (SPS) at 400°C temperature at 50 MPa for 10 min. For simplicity, the samples are indicated as CNF-0, CNF-0.05, CNF-0.1, CNF-0.2 according to the CNF wt.% in the BST matrix. The thermoelectric properties measured in between 300-500 K range. Thermal diffusivity (D) was measured by laser flash method using a 10 mm square sample under 300-500 K and correspondingly specific heat (c) also measured. The density (ρ) was measured using Archimedes principle. Correspondingly, the thermal conductivity (κ) was measured by the product of thermal diffusivity, specific heat, and density. The bulk phase analysis was carried out using X-ray diffraction technique with 10-80° range. The carbon nanofiber (CNF) in bulk composited was analyzed using Raman spectroscopy at room temperature. The morphology and microstructure were observed with scanning electron microscope (SEM). Vickers hardness test was performed on a bulk sample.

2. Results and discussion

Fig. 1 displays the SEM morphology images, XRD and Raman spectroscopy analysis. As seen in Fig. 1(a,b), the BST powder has randomly shaped with a wide particle size and CNF morphology shows elongated cylinder with a diameter

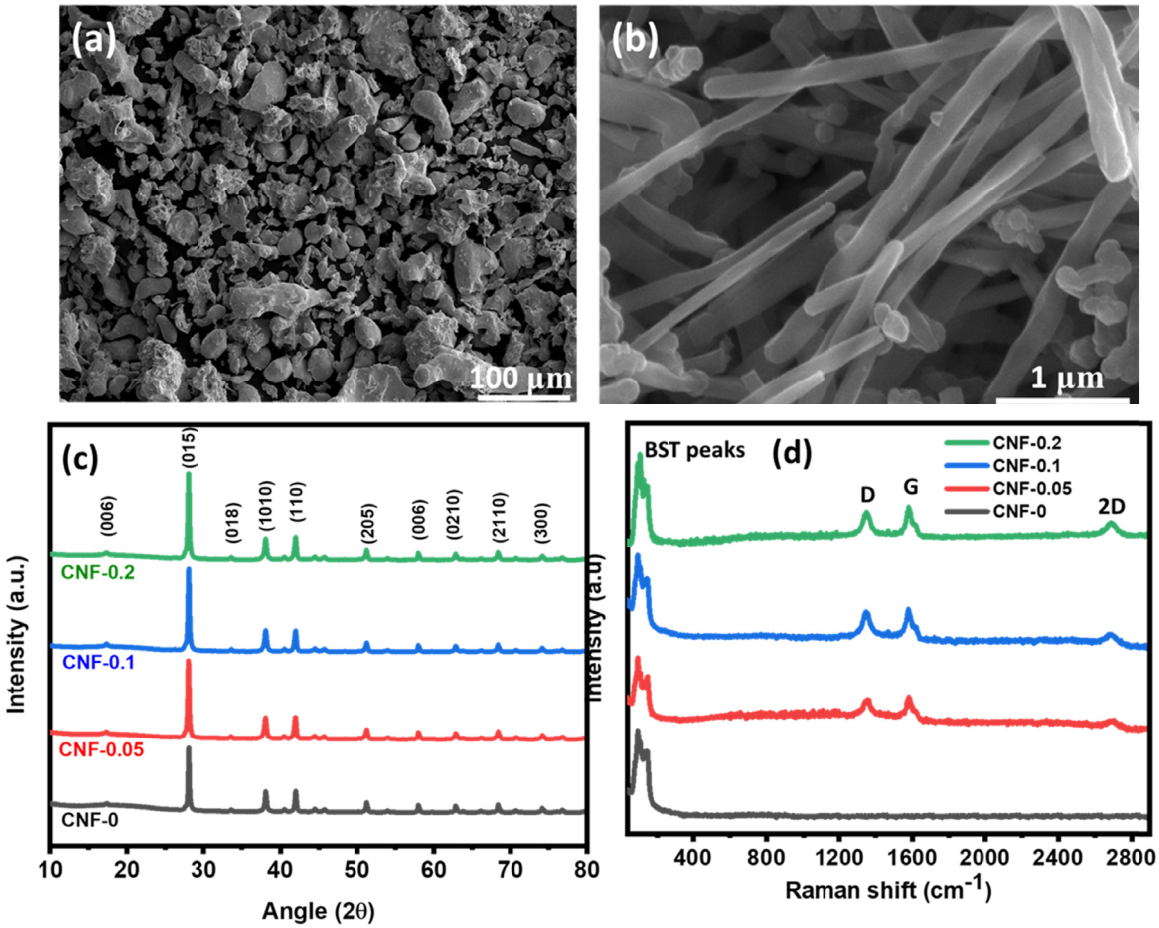

Fig. 1. The scanning electron microscope (SEM) images, (a) water atomized BST powder under 200 μm, (b) elongated carbon nanofiber as a dispersing material in BST matrix, (c) XRD peaks of BST/CNF bulk composites and their corresponding planes, and (d) room temperature Raman spectroscopy of bulk composites; lower and higher wavenumbers represents BST, CNF Raman spectral lines

in nanometer range. The XRD patterns in Fig. 1(c) confirms the bulk BST phase (JCPDS: 00-043-1530) and regardless of CNF, all shows a similar XRD pattern. The CNF related XRD peaks were not observed due to minimal wt.% in the matrix. Raman spectroscopy is an effective tool to elucidate the carbon in composite materials and analyzed results shown in Fig. 1(d). CNF Raman peaks clearly identified and found as D, G and 2D bands, respectively and confirms the presence of CNF in the BST matrix. The observed CNF peaks were consistent with reported literature [16,18].

Fig. 2 represents the SEM images of fracture surface of BST/CNF composites with varying CNF content. The grains were fully dense and obtained relative density above 99% (See Table 1). The grains were randomly dispersed with grain size in micron range. As closely monitored, the significant differences in grain size were clearly visible with increasing CNF content. Noteworthy that grain size was sharply suppressed with CNF content, which was due to the Zener pinning effect [9,19]. The similar behavior of grain size reduction was observed upon the distribution of secondary phases such as Y_2O_3 [9], B_4C [19]. Therefore, it is anticipated to control the grain size of BST matrix through CNF dispersion and concurrently enhancing the mechanical properties.

TABLE 1

Room temperature measured thermoelectric variables; relative density, Lorenz number*10^{-8} ($W\Omega K^{-2}$), effective mass (m^*/m_o), reduced Fermi energy (η), and Vickers hardness (Hv) of BST/CNF composites by varying CNF weight percentage

	CNF-0	**CNF-0.05**	**CNF-0.1**	**CNF-0.2**
Relative density	99.7	99.59	99.24	99.13
Lorentz number	1.667	1.669	1.673	1.673
Effective mass	0.897	0.905	0.919	0.924
Reduced Fermi	–0.509	–0.525	–0.556	–0.562
Vickers hardness (Hv)	80.12	86.74	94.88	101.8

Fig. 3 shows the temperature variation of electrical conductivity, Hall measurement, Seebeck coefficient and power factor of CNF dispersed BST composites, respectively. In Fig. 3(a), electric conductivity (σ) monotonically decreases with temperature and shows the metallic behavior. The σ nature specifies degenerate behavior of BST does not change with addition of CNF. Notable difference with CNF dispersion was found in σ value, as the values undergo decreasing with CNF content and reached 485.6 $\Omega^{-1}cm^{-1}$ with CNF-0.2 sample. To find out conductivity versus CNF trend, room temperature Hall measurement performed and shown in Fig. 3(b). As depicted,

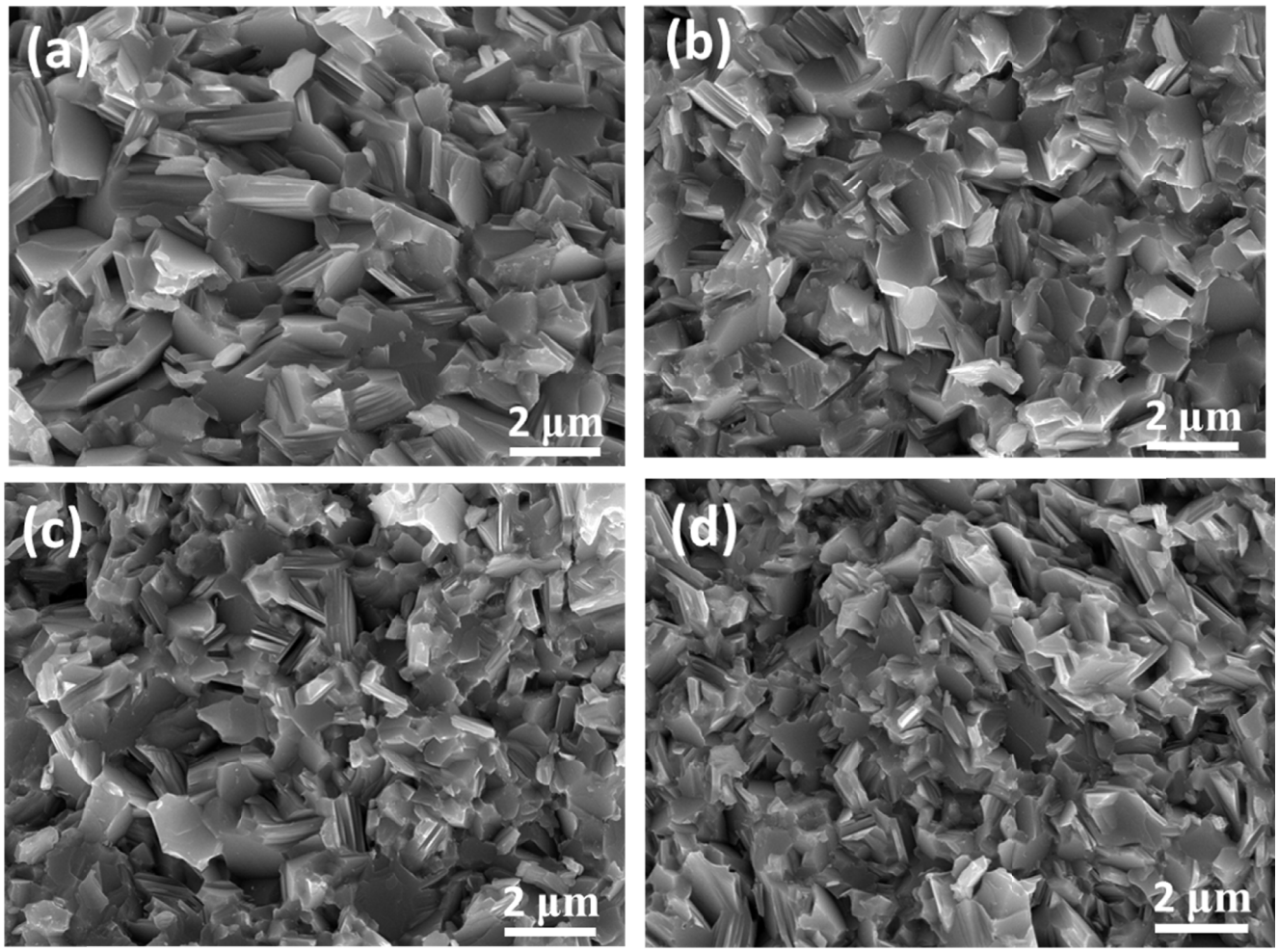

Fig. 2. SEM micrographs of BST/CNF bulk composite fracture surfaces consolidated by spark plasma sintering with varying CNF wt.% in the BST matrix (a) 0 wt.% CNF, (b) 0.05 wt.% CNF, (c) 0.1 wt.% CNF, and (d) 0.2 wt.% CNF samples, respectively

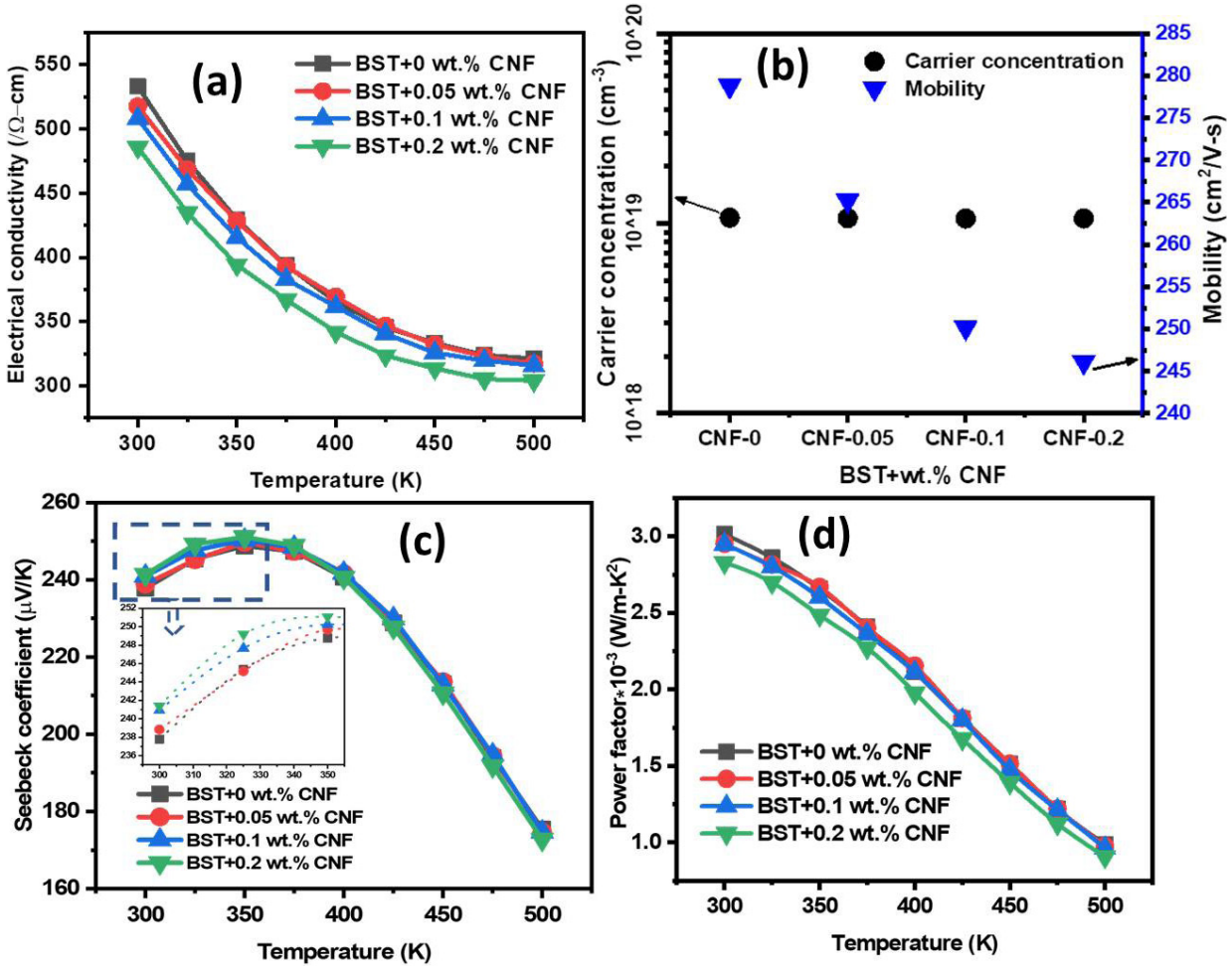

Fig. 3. The temperature dependent (300-500 K) thermoelectric properties, (a) electrical conductivity ($\Omega^{-1}cm^{-1}$), (b) room temperature carrier concentration (cm^{-3}) and mobility ($cm^2/V–s$), (c) Seebeck coefficient (μV/K) (inset picture shows the Seebeck coefficient variation among the samples), and (d) power factor ($W/m–K^2$) of BST/CNF bulk composites

the carrier concentration was consistent in all composites, while the mobility decreased with CNF. The reduction of mobility well-matches with grain size reduction observed in Fig. 2. As the grain size reduces, the density of the grain boundaries raises leads to enhance the carrier scattering, which strongly diminishes mobility values. The carbon atoms in curved graphene sheets form as CNF and they are SP^2 hybridized [13-16]. If the carbon hybridization altered with oxygen, it acts as an insulator [20]. It is anticipated that carbon atoms reacted with oxides available in water atomized BST powder. This might be reason for the unchanged carrier concentration in all samples.

Temperature dependent Seebeck coefficient in BST/*x*-CNF bulk samples were shown in Fig. 3(c). All values were in positive sign and confirmed p-type BST materials. It is noticed that Seebeck coefficient values slightly varied among them and could be observed in the inset picture of Fig. 3(c). The unchanged carrier concentration could be the responsible for the unaltered Seebeck coefficient. Meanwhile, the highest Seebeck values were obtained for 0.2 wt.% dispersed CNF sample. The similar behavior of unaltered Seebeck values also observed upon the dispersion of B_4C into the BiTe matrix [19]. Further understanding of Seebeck coefficient behavior, we estimated band parameters such as effective mass (m^*/m^o) and reduced fermi level (η) using the SPB models [9,21]. There were no severe fluctuations upon the addition of CNF into BST, could be responsible for the unchanged Seebeck coefficient values. The changes in power factor with temperature was displayed in Fig. 3(d). The CNF-0 sample obtained the highest power factor at 300 K with its high electrical conductivity value. The mobility influenced conductivity affects the power factor of BST/CNF composites.

Fig. 4 shows the thermal conductivity (κ) and its lattice (κ_L) and electronic (κ_e) thermal components. As observed in Fig. 4(a), the total thermal conductivity of BST alloy was strongly reduced along with CNF content (See inset picture) as a secondary phase. The value decreased from 1.06 to 0.94 W/m–K about 11% reduction achieved in CNF-0.2 sample. The κ value decrement with CNF dispersion is realized, while constant and higher κ values were reported with CNT, CNF and B_4C dispersed thermoelectric materials [19,22, 23]. Meanwhile, to identify the role of κ_e and κ_L with total κ, we estimated the κ_e utilizing $\kappa_e = L_0\sigma T$, where L_0 is Lorenz number estimated using equations in literatures [9,21] and shown in Fig. 4(b). As predicted with σ value, lowest κ_e value produced in CNF-0.2 sample. The phonon component (κ_L) to total thermal conductivity (κ) was calculated by $\kappa_L = \kappa - \kappa_e$

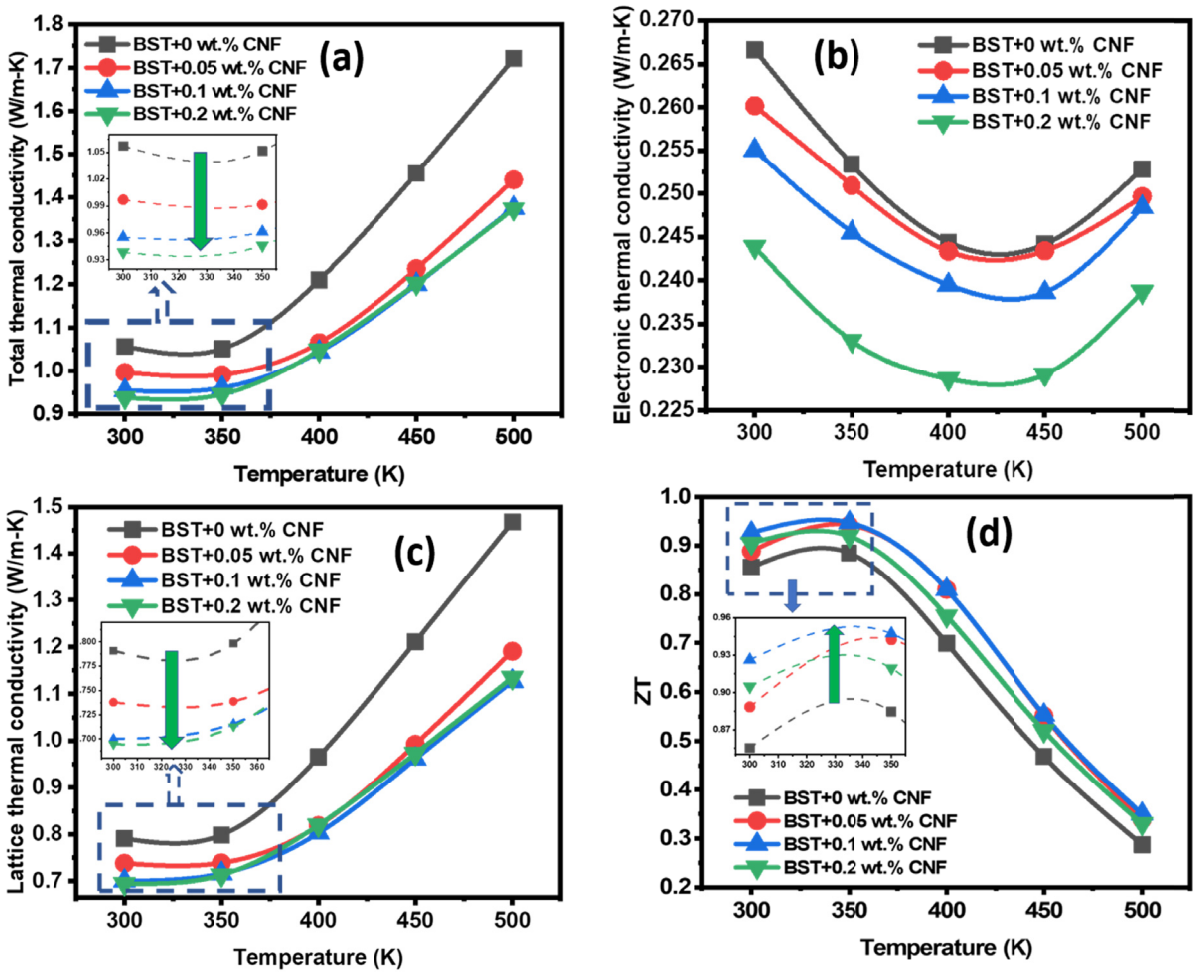

Fig. 4. Thermal transport properties as a function of temperature (a) total thermal conductivity (κ), (b) electrical thermal conductivity (κ_e), (c) lattice thermal conductivity (κ_L), and (d) dimensionless figure of merit (ZT) of bulk BST/CNF composites accordingly with CNF wt.% (the inset pictures in Fig. 4(a,b,d) shows the value differences among the samples)

and plotted in Fig. 4(c). As observed in κ, lattice thermal conductivity (κ_L) was also consistently reduced by increasing CNF percentage in BST matrix. Therefore, it is speculated that κ was strongly influenced by κ_L value. Compared to CNF-0 sample, about 14% decreased κ_L was acquired in CNF-0.2 sample. Minimized κ_L values was observed at 300, 350 K and after instantly exceeded due to bipolar excitation [19-22]. The high dense grain boundaries enhance phonon scattering, and strongly reduced lattice thermal conductivity. The CNF containing samples shows lower κ_L values at high temperatures suggests that CNF shows impact on reducing bipolar excitation.

Fig. 4(d) displays the temperature dependence (300-500 K) of dimensionless figure of merit (ZT). The enhancement of ZT value with CNF was clear, obtained highest ZT of 0.95 seen in CNF-0.1 sample. Identification of ZT variation could be found in the inset picture of Fig. 4(d). The grain boundary modification with reduced thermal conductivity assists in enhanced ZT even though with reduced power factor. Improvement of ZT with CNF is realized, while Quentin et al. [23] reported decreased values in BST/CNT composites. Improving the mechanical properties of BST material is crucial due to cutting waste goes about 50% [24] during module fabrication. The value improved (see Table 1) from 80.12 to 101.8 Hv about 27% enhancement compared to bare sample mainly due to the dispersion strengthening mechanism. The hardness increment with enhanced ZT with BST/CNF composite indicates CNF is a viable secondary phase in BST material.

3. Conclusion

The BST/CNF composites were prepared by combining water atomization and mechanical milling techniques. CNF dispersion effect on thermoelectric properties were investigated and interesting results were evaluated. The microstructure was modified with reduction of grain size simultaneously with CNF content. The unaltered Seebeck coefficient with reduced electrical conductivity decreased the final power factor of composite bulks. However, grain size decrement strongly reduced the total and lattice thermal conductivity due to severe phonon scattering. Altogether, CNF improved the overall ZT value with optimum power factor and reduced thermal values. The mechanical properties were greatly enhanced and attains Vickers hardness of 102 Hv about 27% improvement.

Acknowledgement

This work was supported by the research grant of the Kongju National University in 2020.

REFERENCES

[1] J.R. Szczech, J.M. Higgins, S. Jin, Enhancement of the thermoelectric properties in nanoscale and nanostructured materials, J. Mater. Chem. **21** (12), 4037-4055 (2011).

[2] Y. Pei, X. Shi, A. Lalonde, H. Wang, L. Chen, G.J. Synder, Convergence of electronic bands for high performance bulk thermoelectrics, Nature **473**, 66-69 (2011).

[3] R. Deng, X. Su, S. Hao, Z. Zheng, M. Zhang, H. Xoe, W. Liu, Y. Yan, C. Wolverton, C. Uher, M.G. Kanatzidis, X. Tang, High thermoelectric performance in $Bi_{0.46}Sb_{1.54}Te_3$ nanostructured with ZnTe, Energy Environ. Sci. **11**, 1520-1535 (2018).

[4] H. Mamur, M.R.A Bhuiyan, F. Korkmaz, M. Nil, A review on bismuth telluride (Bi_2Te_3) nanostructure for thermoelectric applications, Renew. Sust. Energ. Rev. **82**, 4159-4169 (2018).

[5] I. Chowdhury, R. Prasher, K. Lofgreen, G. Chrysler, S. Narasimhan, R. Mahajan, R. Venkatasubramanian, On-chip cooling by superlattice-based thin-film thermoelectrics, Nat. Nanotechnol. **4** (4), 235-238 (2009).

[6] Z. Xiao, X. Zhu, On-Chip Sensing of Thermoelectric Thin Film's Merit, Sensors **15** (7), 17232-17240 (2015).

[7] X. Hu, X. Fan, B. Feng, D. Kong, P. Liu, R. Li, Y. Zhang, G. Li, Y. Li, Microstructural refinement, and performance improvement of cast n-type $Bi_2Te_{2.79}Se_{0.21}$ ingot by equal channel angular extrusion, Met. Mater. Int. (2020). https://doi.org/10.1007/s12540-020-00699-5

[8] M. Sabarinathan, M. Omprakash, S. Harish, M. Navaneethan, J. Archana, S. Ponnusamy, Y. Hayakawa, Enhancement of power factor by energy filtering effect in hierarchical $BiSbTe_3$ nanostructures for thermoelectric applications, Appl. Surf. Sci. **418**, 246-251 (2017).

[9] B. Madavali, H.S. Kim, K.H. Lee, S.J. Hong, Enhanced Seebeck coefficient by energy filtering in Bi-Sb-Te based composites with dispersed Y_2O_3 nanoparticles, Intermetallics **82**, 68-75 (2017).

[10] J. Hu, B. Liu, H. Subramanyan, B. Li, J. Zhou, J. Liu, Enhanced thermoelectric properties through minority carriers blocking in nanocomposites, J. Appl. Phys. **126** (9), 095107 (2019).

[11] S. Foster, N. Neophytou, Effectiveness of nano inclusions for reducing bipolar effects in thermoelectric materials, Comput. Mater. Sci. **164**, 91-98 (2019).

[12] L.D. Hicks, T.C. Harman, X. Sun, M.S. Dresselhaus, Experimental study of the effect of quantum-well structures on the thermoelectric figure of merit, Phys. Rev. B **53** (16), R10493-R10496 (1996).

[13] I.V. Zaporotskova, N.P. Boroznina, Y.N. Parkhomenko, L.V. Kozhitov, Carbon nanotubes: Sensor properties, A review, Mod. Electron. Mater. **2** (4), 95-105 (2016).

[14] P.A. Tran, L. Zhang, T.J. Webster, Carbon nanofibers and carbon nanotubes in regenerative medicine, Adv. Drug Deliv. Rev. **61** (12), 1097-1114 (2009).

[15] M. Gurbuz, T. Mutuk, P. Uyan, Mechanical, Wear and Thermal behaviors of graphene reinforced titanium composites, Met. Mater. Int. (2020). https://doi.org/10.1007/s12540-020-00673-1

[16] D.W. Jung, J.H. Jeong, B.C. Cha, J.B. Kim, B.S. Kong, J.K. Lee, E.S. Oh, Effects of ball-milled graphite in the synthesis of SnO_2/graphite as an active material in lithium-ion batteries, Met. Mater. Int. **17** (6), 1021-1026 (2011).

[17] A comparison of Carbon Nanotubes and Carbon Nanofibers, Pyrograf products, Inc, An affiliate of Applied surface sciences, Inc.

[18] K.M. Nam, K. Mees, H.S. Park, M. Willert-Porada, C.S. Lee, Electrophoretic Deposition for the Growth of Carbon nanofibers on Ni-Cu/C-fiber Textiles, Bull. Korean Chem. Soc. **35** (8), 2431-2437 (2014).

[19] S.J. Jung, S.Y. Park, B.K. Kim, B. Kwon, S.K. Kim, H.H. Park, S.H. Baek, Hardening of Bi-Te based alloys by dispersing B_4C nanoparticles, Acta Mater. **97**, 68-74 (2015).

[20] C. Marquez, N. Rodriguez, R. Ruiz, F. Gamiz, Electrical characterization and conductivity optimization of laser reduced graphene oxide on insulator using point-contact methods, RSC Adv. **6** (52), 46231-46237 (2016).

[21] P. Sharief, B. Madavali, J.M. Koo, H.J. Kim, S. Hong, S.J. Hong, Effect of milling time parameter on the microstructure and the thermoelectric properties of N-type $Bi_2Te_{2.7}Se_{0.3}$ alloys, Arch. Metall. Mater. **2**, 585-590 (2019).

[22] P. Slobodian, P. Riha, R. Olejnik, M. Kovar, P. Svoboda, Thermoelectric properties of carbon nanotube and nanofiber based ethylene-octene copolymer composites for thermoelectric devices, J. Nanomater 2013, 1-7 (2013).

[23] Q. Lognoné, F. Gascoin, On the effect of carbon nanotubes on the thermoelectric properties of n-$Bi_2Te_{2.4}Se_{0.6}$ made by mechanical alloying, J. Alloys Compd. **635**, 107-111 (2015).

[24] B. Feng, G. Li, X. Hu, P. Liu, R. Li, Y. Zhang, Z. He, Improvement of thermoelectric and mechanical properties of BiCuSeO-based materials by SiC nanodispersion, J. Alloys Compd. **818**, 152899 (2020).